




## Magnetic-order-induced ferroelectric polarization in the polar antiferromagnets $R\text{FeWO}_6$ ( $R = \text{Sm}, \text{Gd}, \text{Er}, \text{and Tm}$ )

Premakumar Yanda , Swarnamayee Mishra, and A. Sundaresan \*

*School of Advanced Materials, and Chemistry and Physics of Materials Unit, Jawaharlal Nehru Centre for Advanced Scientific Research, Jakkur, Bangalore – 560064, India*

 (Received 22 April 2021; accepted 30 June 2021; published 15 July 2021)

We report the synthesis, structure, and magnetism-induced multiferroic properties of the polar magnets  $R\text{FeWO}_6$  ( $R = \text{Tm}, \text{Sm}, \text{Gd}, \text{and Er}$ ). All these compounds crystallize in the orthorhombic structure with the polar symmetry  $Pna2_1$ , which results from the ordering of  $\text{Fe}^{3+}$  and  $\text{W}^{6+}$  ions at different crystallographic sites. DC magnetization and specific heat measurements confirm the antiferromagnetic order of  $\text{Fe}^{3+}$  spins at  $T_{N1} = 14\text{--}18$  K and magnetic ordering of  $R$  ions at low temperatures. The magnetic order of  $\text{Fe}^{3+}$  ions in these compounds is accompanied by a dielectric anomaly and a change in electric polarization. Intriguingly, a second ferroelectric transition occurs at the magnetic ordering temperature ( $T_{N2} = 5.5$  K) of  $\text{Tm}^{3+}$  ions in  $\text{TmFeWO}_6$ . The magnetic field dependent behavior of electric polarization varies with  $R$  ion, indicating the coupling between  $4f\text{--}3d$  spins. The emergence of change in ferroelectric polarization at the magnetic ordering temperatures demonstrates the multiferroic nature of the polar magnets  $R\text{FeWO}_6$  ( $R = \text{Tm}, \text{Sm}, \text{Gd}, \text{and Er}$ ). Our study indicates that the aeschynite type family of compounds with polar symmetry can be an excellent platform to understand the role of  $4f\text{--}3d$  coupling on multiferroicity.

DOI: [10.1103/PhysRevMaterials.5.074406](https://doi.org/10.1103/PhysRevMaterials.5.074406)

### I. INTRODUCTION

Multiferroics are magnetic insulators that exhibit a coupled ferroelectric polarization and magnetization. They have attracted attention in the past two decades due to their fascinating physics and potential applications for advanced multifunctional devices [1–10]. However, the contradictory requirements for ferroelectricity and magnetism make it challenging to design single-phase multiferroics [8,11]. Nevertheless, this difficulty has been overcome by creating multiferroics with the different origins of ferroelectricity. Based on the mechanism of ferroelectricity, multiferroics are classified into two types; In *Type-I* multiferroics, ferroelectricity and magnetism occur at different temperatures leading to weak coupling between electric and magnetic orders. On the other hand, *Type-II* multiferroics that exhibit ferroelectric polarization of magnetic origin show strong magnetoelectric coupling. In general, *Type-II* multiferroics are centrosymmetric in the paramagnetic region, and specific magnetic structures break the inversion symmetry, which results in ferroelectricity. Mostly, these magnetic structures are complicated and occur at very low temperatures, which makes these materials challenging to use in applications. Hence, it is essential to find new multiferroic materials with strong magnetoelectric coupling at room temperature.

Recently, polar magnets with polar crystal symmetry and exhibiting magnetic order have drawn much attention to multiferroicity [12–18]. These materials can be classified as a new class of multiferroics since the origin of ferroelectricity

differ from the multiferroics mentioned above. Polar magnets do not need complicated spin structures to show the electric polarization, and hence they have potential for room-temperature multiferroics. There are few reports, and recently there is a perspective on polar magnets as multiferroics in the literature [12,17,18]. These compounds are stabilized in the polar structure by chemical ordering. There are quite a few polar magnetic materials reported to be multiferroics, for example,  $\text{CaBaCo}_4\text{O}_7$ ,  $M_2\text{Mo}_3\text{O}_8$  ( $M = \text{Mn}, \text{Fe}, \text{and Co}$ ),  $\text{Ni}_3\text{TeO}_6$ , corundum derivatives, and doubly ordered perovskites, etc. [12,13,16,19–25]. Recently, another interesting family of compounds  $R\text{FeWO}_6$  ( $R = \text{Dy}, \text{Tb}, \text{Eu}, \text{and Y}$ ) reported to be polar magnets, which are ordered derivatives of the centrosymmetric parent compound, aeschynite- $\text{CaTa}_2\text{O}_6$  and show multiferroic properties [17,26,27]. These compounds crystallize in the orthorhombic structure with polar space group  $Pna2_1$ . The polar distortion arises from the ordering of  $\text{Fe}^{3+}$  and  $\text{W}^{6+}$  ions at different crystallographic sites. They exhibit antiferromagnetic order of  $\text{Fe}^{3+}$  ions at  $T_{N1} = 15\text{--}18$  K, accompanied by a switchable electric polarization, indicating that these compounds are multiferroics. From the neutron diffraction studies, the magnetic structure of  $\text{DyFeWO}_6$  is reported to be (MSG:  $C_{ac}$ ) noncollinear and commensurate with the  $\mathbf{k}$  vector  $(0 \frac{1}{2} \frac{1}{2})$ , which is compatible with observed polarization. Following this study, two other isostructural compounds,  $R\text{CrWO}_6$  ( $R = \text{Y}, \text{Ho}, \text{and Lu}$ ) and  $\text{DyVWO}_6$ , were reported to be polar magnets with a collinear magnetic structure of  $\text{Cr}^{3+}$  sublattice [28–32]. In contrast to  $R\text{FeWO}_6$  ( $R = \text{Dy}, \text{Tb}, \text{Eu}, \text{and Y}$ ), Cr and V based compounds are not multiferroics presumably due to different spin structures that they adapt or the change in polarization is very small to be detected within the limit of our measurement

\*sundaresan@jncasr.ac.in

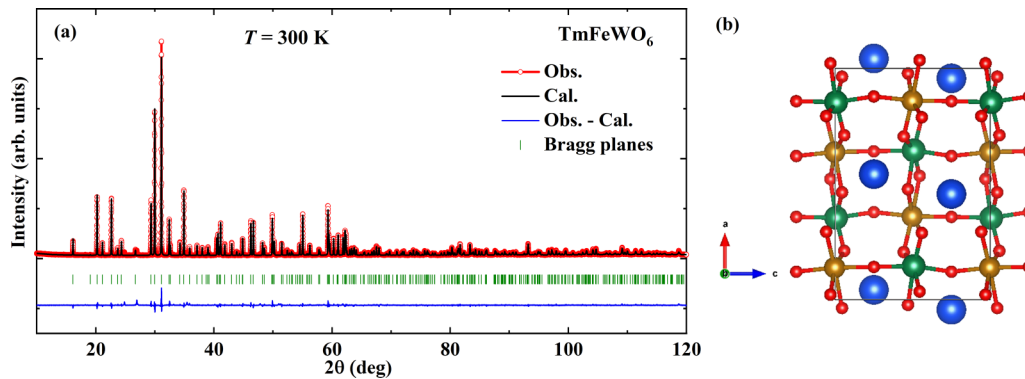


FIG. 1. (a) Rietveld refinement of room temperature XRD data of  $\text{TmFeWO}_6$ . (b) Schematic of the crystal structure of  $R\text{FeWO}_6$  ( $R = \text{Tm}, \text{Sm}, \text{Gd}, \text{and Er}$ ) projected along the  $b$  direction. Rare earth (blue), Iron (brown), Tungsten (green), and Oxygen (red).

( $\sim 0.01 \mu\text{C}/\text{m}^2$ ). Besides, the  $4f-3d$  interactions seem to play a role in the multiferroic properties like those observed in the manganites, orthoferrites, and green phase compounds [3,5,33–36]. Along this line, we have studied the other members of  $R\text{FeWO}_6$ , to understand the effect of rare-earth on the multiferroic properties.

In this article, we report the synthesis and characterization of polar magnets  $R\text{FeWO}_6$  ( $R = \text{Tm}, \text{Sm}, \text{Gd}, \text{and Er}$ ) that are isostructural to  $\text{DyFeWO}_6$  [17]. All these compounds crystallize in the orthorhombic  $Pna2_1$  crystal structure, an ordered derivative of the centrosymmetric parent compound  $\text{CaTa}_2\text{O}_6$  [27]. They exhibit an antiferromagnetic ordering of  $\text{Fe}^{3+}$  ions at  $T_{N1} = 14-18$  K. Isothermal magnetization curves reveal the metamagnetic transitions at a critical field. A change in polarization observed at the magnetic ordering temperature  $T_{N1}$  demonstrates that these compounds are multiferroics. Interestingly,  $\text{TmFeWO}_6$  shows a second ferroelectric transition below  $T_{N2} = 5.5$  K where  $\text{Tm}^{3+}$  ions order independently. The ferroelectric polarization in these polar magnets is greatly affected by the applied magnetic field, demonstrating a strong magnetoelectric coupling.

## II. EXPERIMENTAL SECTION

Polycrystalline samples of  $R\text{FeWO}_6$  ( $R = \text{Tm}, \text{Sm}, \text{Gd}, \text{and Er}$ ) were prepared by the conventional solid-state reaction method. Stoichiometric amounts of  $R\text{FeO}_3$  and  $\text{WO}_3$  powders were mixed well and heated in the temperature range

1050–1100 °C for 24 h in evacuated and sealed quartz tubes with intermittent grindings. Powder x-ray diffraction (XRD) data were collected at room temperature with a PANalytical Empyrean alpha-1 diffractometer using monochromatic  $\text{Cu K}\alpha_1$  radiation and analyzed using FULLPROF [37]. DC magnetization measurements were carried out using a Superconducting Quantum Interference Device Magnetometer (Quantum Design, USA). Specific heat measurements were performed in the Physical Property Measurement System, Quantum Design, USA. Dielectric measurements were carried out on disc-shaped pellets with silver electrodes on either side using an Agilent E4980A LCR meter. The dimensions of each sample are provided in the Supplemental Material [38]. A Keithley electrometer is used to record the pyrocurrent, DC bias current, and the polarization was obtained by integrating pyrocurrent with respect to time.

## III. RESULTS AND DISCUSSIONS

Figure 1(a) shows Rietveld refined XRD pattern of  $\text{TmFeWO}_6$  obtained at the final cycle of the refinement, and the obtained structural parameters are provided in Table I. The results of refinements of all other compounds and their structural parameters are provided in the Supplemental Material [38]. These samples contain minor impurity phases, such as garnet,  $R_6\text{WO}_{12}$ , and  $\text{Fe}_3\text{O}_4$ . We have realized that it requires a synchrotron or neutron diffraction to get accurate positional parameters for all the compounds reported here. However, our

TABLE I. Crystallographic structural parameters of  $\text{TmFeWO}_6$  obtained from the refinement of room temperature XRD data.

| Atom | Wyckoff Position | $x$        | $y$        | $z$        | $B_{\text{iso}} (\text{\AA}^2)$ | Occu. |
|------|------------------|------------|------------|------------|---------------------------------|-------|
| Tm   | 4a               | 0.0435(2)  | 0.4575(6)  | 0.25       | 0.789(68)                       | 1     |
| Fe   | 4a               | 0.1387(9)  | 0.9659(15) | 0.9870(32) | 0.176(52)                       | 1     |
| W    | 4a               | 0.3532(3)  | 0.4503(6)  | 0.0046(12) | 0.844(60)                       | 1     |
| O1   | 4a               | 0.9732(31) | 0.7782(70) | 0.0523(63) | 1                               | 1     |
| O2   | 4a               | 0.5389(30) | 0.2609(67) | 0.9685(73) | 1                               | 1     |
| O3   | 4a               | 0.2031(31) | 0.6416(66) | 0.0672(46) | 1                               | 1     |
| O4   | 4a               | 0.2875(31) | 0.1029(74) | 0.9399(47) | 1                               | 1     |
| O5   | 4a               | 0.1593(26) | 0.0685(56) | 0.2448(59) | 1                               | 1     |
| O6   | 4a               | 0.1132(24) | 0.8366(55) | 0.7679(64) | 1                               | 1     |

Space group:  $Pna2_1$ ;  $a = 10.9738(2) \text{\AA}$ ,  $b = 5.1371(1) \text{\AA}$ ,  $c = 7.3095(1) \text{\AA}$ ,  $\alpha = \beta = \gamma = 90^\circ$ ,  $V = 412.063(11) \text{\AA}^3$ ;  $\chi^2 = 3.62$ ,  $R_{\text{Bragg}} (\%) = 5.44$ ,  $R_f (\%) = 4.72$ .

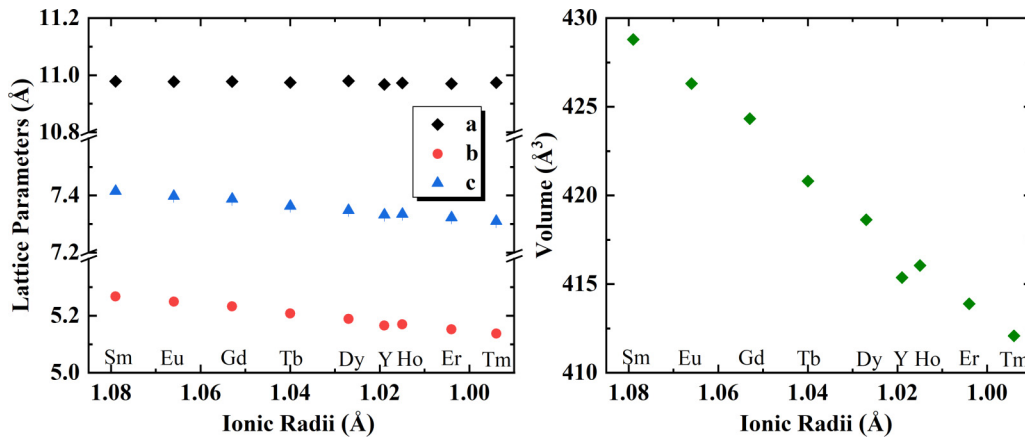


FIG. 2. Variation of the lattice parameters  $a$ ,  $b$ , and  $c$  vs ionic radii and the unit cell volume for different  $R\text{FeWO}_6$  compounds. We have taken the values for Dy, Eu, Tb, Y from Ref. [17] and Ho from Ref. [39].

refinement confirms that all the four compounds crystallize in the polar orthorhombic structure with space group  $Pna2_1$  [17]. The chemical ordering of  $\text{Fe}^{3+}$  and  $\text{W}^{6+}$  ions in the parent aeschynite structure (space group:  $Pnma$ ) breaks the inversion center and results in the polar structure [27]. The schematic of the crystal structure of  $R\text{FeWO}_6$  ( $R = \text{Tm}$ , Sm, Gd, and Er) is shown in Fig. 1(b). We can see from this figure that the three-dimensional structure is formed by connecting the corners of  $\text{FeO}_6$  and  $\text{WO}_6$  edge shared octahedra dimers. The rare-earth ions are located in the tunnels to form  $RO_8$  polyhedra. As shown in Fig. 2, the lattice parameters  $b$ ,  $c$ , and volume of unit cell decrease linearly as a function of the radius of lanthanide ion while going from Sm to Tm. On the other hand, the parameter  $a$  remains almost constant. We have also collected the XRD data of  $\text{GdFeWO}_6$  at  $800^\circ\text{C}$ , as shown in Fig. S4, confirming that there is no structural transition, and the polar structure might be stable up to the formation or decomposition temperatures of all these compounds [38]. In the following sections, we will present the physical properties of all these compounds.

### A. $\text{TmFeWO}_6$

Temperature-dependent susceptibility and specific heat of  $\text{TmFeWO}_6$  are given in Fig. 3(a). It is apparent from this figure that the heat capacity exhibits anomalies corresponding to the magnetic ordering of  $\text{Fe}^{3+}$  ions at  $T_{N1} = 14.5$  K and independent order of  $\text{Tm}^{3+}$  ions at  $T_{N2} = 5.5$  K. From the Curie-Weiss fit to inverse susceptibility (see Fig. S5), the obtained value of the effective paramagnetic moment is  $9.965 \mu_B$ , which is in good agreement with the theoretical value  $9.602 \mu_B$  for both  $\text{Tm}^{3+}$  and  $\text{Fe}^{3+}$  ions and the Curie-Weiss temperature  $\theta_{CW} = -38.5$  K [38]. The negative sign indicates that the dominant interactions are antiferromagnetic. However, the  $\theta_{CW}$  is high as compared to the  $T_{N1}$  suggesting that the system is moderately frustrated. We did not observe any signs of ordering in the magnetic susceptibility at  $T_{N1}$ . This is because the susceptibility is dominated by the large paramagnetic moment of  $\text{Tm}^{3+}$  ions. From the inset of Fig. 3(a), the linear behavior of field-dependent isothermal magnetization at  $T > T_{N2}$  is as expected for the antiferromagnetic ordering. However, below  $T_{N2}$ , this compound exhibits

a metamagnetic transition with a critical field of about 1 T. This field-induced transition develops with the hysteresis in isothermal magnetization (Fig. S6), indicating the first-order nature of the metamagnetic transition [38].

Figure 3(b) presents the results of dielectric measurements on  $\text{TmFeWO}_6$ . The dielectric anomaly, observed at  $T_{N1}$ , is nearly independent of applied magnetic fields, and there is a broad anomaly around  $T_{N2}$ . This anomaly starts well above the transition and is suppressed under applied magnetic fields, indicating the coupling between magnetic and dipole orders in this compound. The dissipation factor, as shown in the inset of Fig. 3(b), shows similar behavior as the dielectric constant. The observed dielectric anomalies did not shift with the frequency (Fig. S7), which excludes any extrinsic effects and confirms its magnetic origin [38]. However, we have observed dispersion of dielectric curves in the measured temperature range, indicating the presence of dielectric relaxation that can be of Maxwell-Wagner type. Also, this compound shows the magnetodielectric effect of 2% at 2 K and 9 T, as seen in Fig. S8 [38].

To examine whether these dielectric anomalies are associated with ferroelectricity or not, we have recorded the pyrocurrent behavior across the magnetic ordering temperatures. Following the observed dielectric anomalies, we observe two pyrocurrent anomalies in the same direction at both  $T_{N1}$  and  $T_{N2}$ , implying two ferroelectric (FE) transitions which can be seen in Fig. S9 [38]. The second ferroelectric transition is absent in the isostructural compounds  $R\text{FeWO}_6$  ( $R = \text{Dy}$ , Eu, Tb, and Y) [17]. The change in polarization ( $\Delta P$ ) below the magnetic ordering obtained by integrating the pyrocurrent with respect to time and its magnetic field dependence is shown in Fig. 3(c). As seen from the inset of Fig. 3(c), the change in polarization in the FE1 region is almost unchanged under the applied magnetic field. In contrast, the change in polarization below FE2 is four times higher than that of FE1 under zero field and suppressed with the applied magnetic field. The maximum change in polarization is  $\sim 0.4 \mu\text{C}/\text{m}^2$  in the FE1 region and  $\sim 1.8 \mu\text{C}/\text{m}^2$  in the FE2 region at 2 K under zero magnetic field. The  $\Delta P$  can be switched by changing the direction of the poling electric field, as seen from Fig. 3(c). It is known that DC bias measurement is a valuable tool to find out the intrinsic nature of ferroelectric

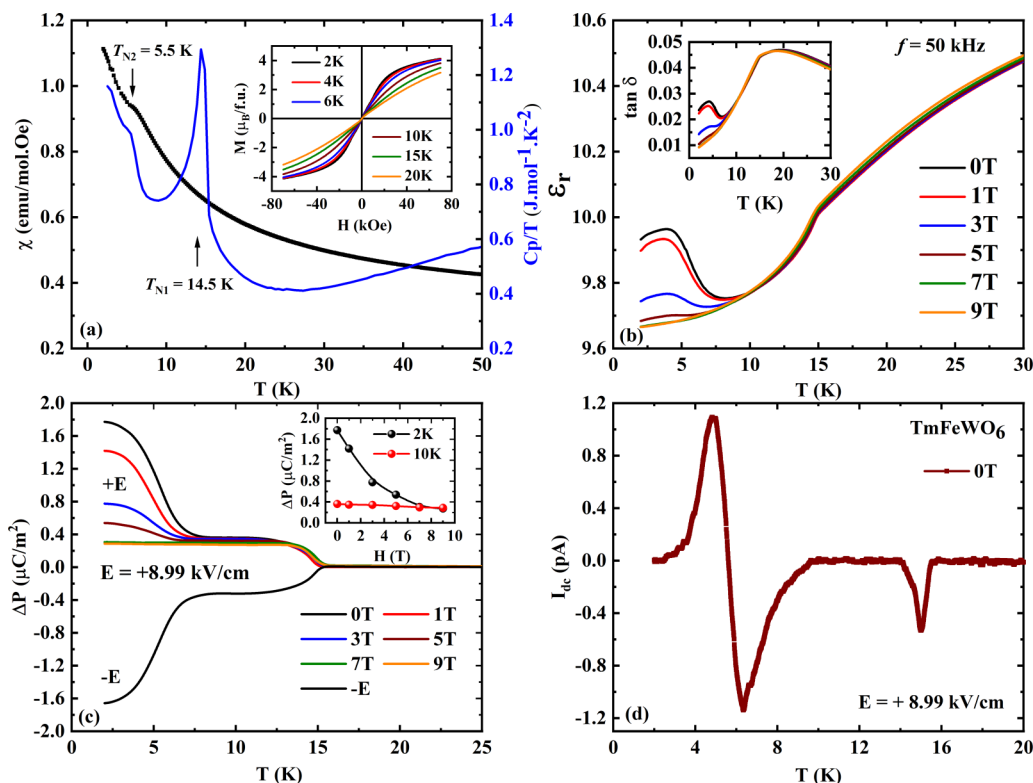


FIG. 3. (a) Left axis. Variation of DC susceptibility with temperature in TmFeWO<sub>6</sub> measured under 0.01 T. Right axis. Heat capacity measured under 0 T. Inset shows the isothermal magnetization curves at different temperatures. (b) Temperature-dependent dielectric constant measured under various magnetic fields at the frequency  $f = 50$  kHz. Inset shows the corresponding loss behavior. (c) Temperature and magnetic field-dependent change in polarization and its switching. Inset.  $\Delta P$  vs  $H$  behavior at 2 and 10 K. (d) DC bias signal recorded across the ferroelectric transition under 0 T.

polarization [40,41]. The inherent nature of the ferroelectricity is further supported by the DC bias measurement, which is given in Fig. 3(d). The presence of two DC bias signals at the magnetic transitions evidence the FE transitions. The change in polarization in the FE2 region is started well above the  $T_{N2}$ , similar to the dielectric behavior. Later, we will discuss this behavior in comparison with the other compounds. A schematic  $H$ - $T$  phase diagram of TmFeWO<sub>6</sub> is shown in Fig. 4 where we can see the two ferroelectric transitions and their field dependence.

### B. SmFeWO<sub>6</sub>

In Fig. 5(a), the temperature-dependent susceptibility of SmFeWO<sub>6</sub> shows the anomaly around  $T_{N1} = 16.3$  K indicating the antiferromagnetic ordering of Fe<sup>3+</sup> ions. The susceptibility increases below  $T_{N1}$  due to the paramagnetic moment contribution of Sm<sup>3+</sup> ions. The long-range magnetic ordering is confirmed by the  $\lambda$ -type anomaly in  $C_p(T)$ , as seen in the same figure. The broad hump around 6 K in heat capacity indicates a possible Schottky-type anomaly. Fe spins may polarize the Sm moments below  $T_{N1}$  and the independent magnetic ordering of Sm<sup>3+</sup> ions can occur at  $T_{N2} = 6$  K. However, it requires a neutron diffraction study to confirm this possibility. The magnetic field-dependent isothermal magnetization curves [inset of Fig. 5(a)] are consistent with the antiferromagnetic ordering of SmFeWO<sub>6</sub>. The dielectric anomaly at  $T_{N1}$  indicates the magnetodielectric effect, as seen

from Fig. 5(b). This anomaly is nearly independent of the applied magnetic field but shifts towards lower temperatures as the field increases. Similar behavior is observed for the loss factor, which is shown in the inset of Fig. 5(b). The dielectric constant falls off at low temperatures, and a broad anomaly is observed in the corresponding loss data around 6 K. This change may be due to the independent ordering of Sm<sup>3+</sup> ions.

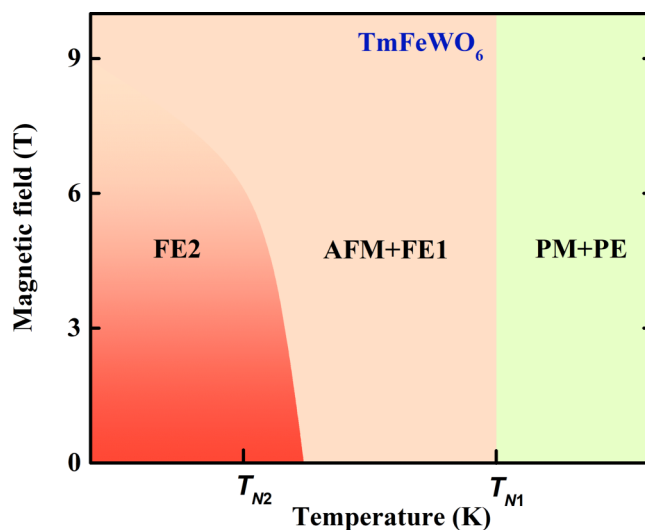


FIG. 4. Schematic  $H$ - $T$  phase diagram for TmFeWO<sub>6</sub>, which shows two ferroelectric transitions.



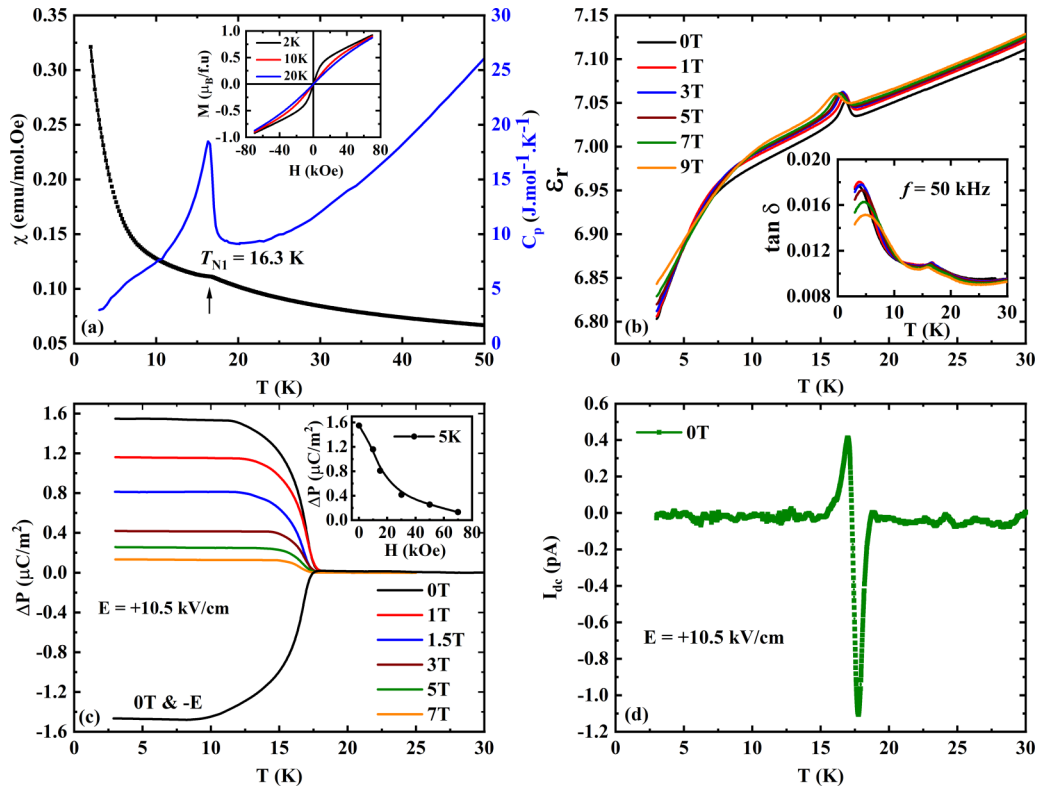


FIG. 5. (a) Left axis. Temperature-dependent dc susceptibility of SmFeWO<sub>6</sub> measured under 0.01 T. Right axis. Specific heat obtained under 0 T. Inset shows  $M$  vs  $H$  curves at different temperatures. (b) Temperature evolution of dielectric constant measured under various magnetic fields with frequency  $f = 50$  kHz. Inset shows the corresponding dissipation factor. (c) Temperature and magnetic field-dependent change in polarization and its switching behavior obtained from pyrocurrent. Inset.  $\Delta P$  vs  $H$  behavior at 5 K. (d) DC bias signal.

Moreover, the frequency-dependent dielectric data which is given in Fig. S10, confirms the magnetodielectric coupling and dielectric relaxation behavior of SmFeWO<sub>6</sub> [38].

The recorded pyrocurrent shows an asymmetric peak at  $T_{N1}$  indicating the appearance of polarization, as shown in Fig. S11 [38]. This peak is suppressed under applied magnetic fields. The corresponding change in polarization and its magnetic field dependence are shown in Fig. 5(c). The change in polarization ( $\Delta P$ ) is maximum with the value  $\sim 1.5 \mu C/m^2$  at 2 K under zero magnetic field and suppressed with increasing applied magnetic fields [see Fig. 5(c)]. The applied magnetic fields can change the ground state magnetic structure and decrease the change in polarization. Further, the electric polarization is switched by changing the direction of the poling electric field [Fig. 5(c)] and DC bias measurement from Fig. 5(d) confirms the intrinsic behavior of the ferroelectricity. These results demonstrate that SmFeWO<sub>6</sub> is multiferroic.

### C. GdFeWO<sub>6</sub>

GdFeWO<sub>6</sub> exhibits antiferromagnetic ordering of Fe<sup>3+</sup> ions at  $T_{N1} = 16.2$  K and Gd<sup>3+</sup> ions order at  $T_{N2} = 5.9$  K, as shown in Fig. 6(a). The effective magnetic moment  $10.175 \mu_B$  obtained from the Curie-Weiss fit (see Fig. S12) is in good agreement with the free ion moment for Gd<sup>3+</sup> and Fe<sup>3+</sup> ions which is  $9.904 \mu_B$  [38]. The Curie-Weiss temperature is  $\theta_{CW} = -27.2$  K indicates the dominant antiferromagnetic interactions. We did not observe the peak at  $T_{N1}$  in susceptibility because of the large contribution from the paramagnetic mo-

ment of Gd<sup>3+</sup> ions. Isothermal magnetization curves, which are given in the inset of Fig. 6(a), show linear behavior supporting the antiferromagnetic ordering below  $T_{N1}$ . The S-type behavior below  $T_{N2}$  indicates the possible metamagnetic transition. The magnetization value observed at 2 K and 7 T is  $\sim 7.9 \mu_B/f.u.$ , which is nearly equivalent to the saturated magnetization  $\sim 8.6 \mu_B/f.u.$ , of both Gd<sup>3+</sup> and Fe<sup>3+</sup> ions. Therefore, the metamagnetic transition associated with Gd<sup>3+</sup> spins is antiferromagnetic to ferromagnetic.

From Fig 6(b), GdFeWO<sub>6</sub> exhibits a dielectric anomaly at  $T_{N1}$ , which became broad under the applied magnetic fields. This effect is evident in loss data where a sharp anomaly is observed at  $T_{N1}$  [see inset of Fig. 6(b)]. These anomalies did not shift with frequency, as shown in Fig. S13, indicating the magnetic origin and cross coupling between magnetic and dielectric orders. The pyrocurrent measurements given in Fig. S14, confirm that this dielectric anomaly is associated with ferroelectricity [38]. The maximum change in polarization ( $\Delta P$ ) is  $5.5 \mu C/m^2$  at 2 K under zero magnetic field, and  $\Delta P$  is suppressed upon increasing the magnetic field [see Fig. 6(c)]. Further, the polarization is switchable [Fig. 6(c)], and DC bias measurements [Fig. 6(d)] confirmed the intrinsic nature of ferroelectricity.

### D. ErFeWO<sub>6</sub>

The results of ErFeWO<sub>6</sub> are presented in Fig. 7 where the antiferromagnetic order of Fe sublattice is seen at  $T_{N1} =$

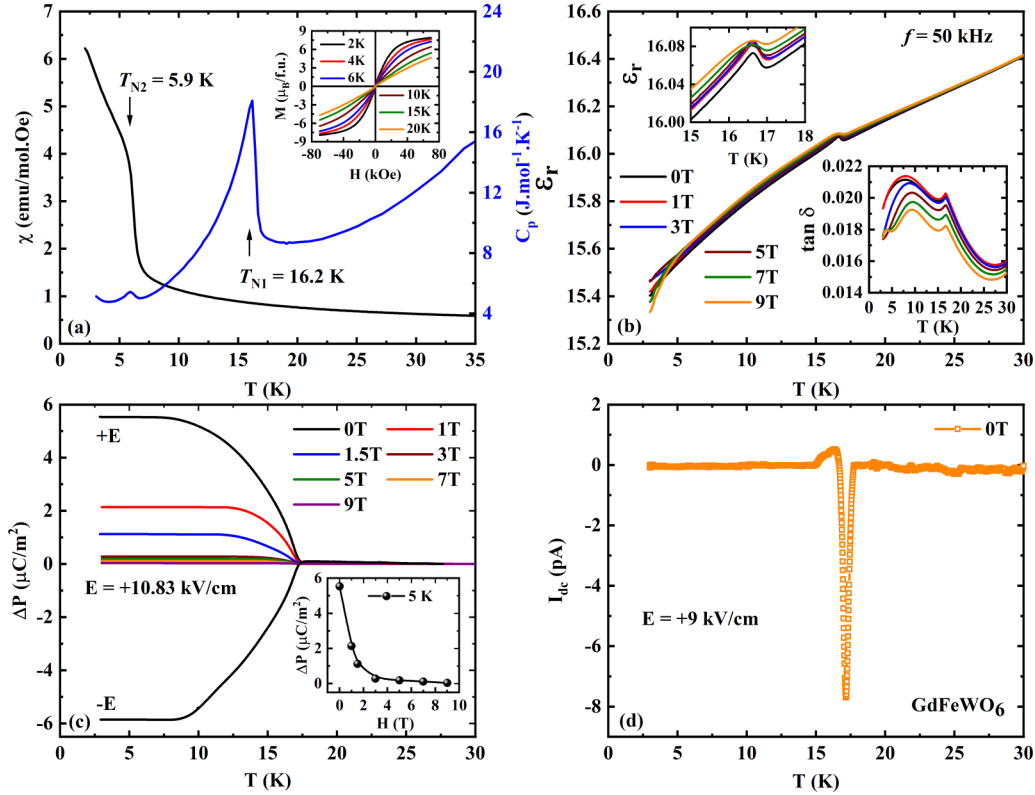


FIG. 6. (a) Left. DC susceptibility against temperature measured under a magnetic field of 0.01 T for GdFeWO<sub>6</sub>. Right.  $C_p$  vs  $T$ . The inset shows  $M$  vs  $H$  plots at different temperatures. (b) Dielectric constant with respect to the temperature recorded under various magnetic fields with frequency  $f = 50$  kHz. Inset. Enlarged view of dielectric constant (left) and loss data (right). (c) Change in polarization under different magnetic fields and switching of polarization with the direction of the poling electric field. The inset shows  $\Delta P$  vs  $H$  at 5 K. (d) DC bias measurement.

15.1 K [Fig. 7(a)], further supported by the anomaly in  $dM/dT$ , as shown in the bottom inset. A clear indication of the antiferromagnetic ordering of the Fe<sup>3+</sup> ions is further confirmed by the heat capacity data given in Fig. 7(a). Also, a Schottky-type anomaly is seen around  $T_{N2} = 4$  K where Er<sup>3+</sup> moments independent ordering might be possible. The Curie-Weiss fit to susceptibility also suggests the presence of Er<sup>3+</sup> and Fe<sup>3+</sup> oxidation states and the presence of antiferromagnetic interactions (see Fig. S15) [38]. Isothermal magnetization curves are linear as expected for the antiferromagnetic ordering and reveal the metamagnetic transition associated with the magnetic Er<sup>3+</sup> ions below  $T_{N2}$ . ErFeWO<sub>6</sub> compound exhibits dielectric anomaly at  $T_{N1}$  which shifts to lower temperatures upon increasing the applied magnetic field as shown in Fig. 7(b). The corresponding loss data shows anomalous behavior at  $T_{N1}$ . The frequency-dependent dielectric data is similar to that of other compounds suggesting the intrinsic nature of magnetodielectric coupling and the presence of dielectric relaxation (see Fig. S16) [38]. The compound shows a magnetodielectric effect of 0.11% at 2 K and 5 T, which can be seen in Fig. S17 [38]. Pyroelectric measurements (see Fig. S18) suggest a change in polarization that occurs below  $T_{N1}$ , as depicted in Fig. 7(c), demonstrating the multiferroic nature of ErFeWO<sub>6</sub> [38]. Unlike the other compounds, the  $\Delta P$  is suppressed completely and becomes zero at high magnetic fields. The maximum change in polarization is  $3.5 \mu\text{C}/\text{m}^2$  at 2 K under zero magnetic fields.

These results are further supported by switching and DC bias measurements, as given in Figs. 7(c) and 7(d).

Finally, we have summarized the magnetic transition temperatures of this aeschynite family of compounds along with the reported ones in Table II. All these compounds exhibit the antiferromagnetic ordering of Fe<sup>3+</sup> ions around  $T_{N1} = 14$ –18 K and rare-earth ions order at low temperatures. However, Fe<sup>3+</sup> ions induce the moment at the rare-earth site indicating the  $4f$  and  $3d$  interactions. As shown earlier, isothermal magnetization measurements reveal metamagnetic transitions associated with the magnetic rare-earth ions. In GdFeWO<sub>6</sub>, the magnetization is almost saturated at 7 T with

TABLE II. The magnetic transition temperatures of  $R\text{FeWO}_6$  compounds.

| $R$ | $T_{N1}$ (K) | $T_{N2}$ (K) | Ref.         |
|-----|--------------|--------------|--------------|
| Sm  | 16.3         | 6            | Present work |
| Eu  | 17           | –            | [17]         |
| Gd  | 16.2         | 5.9          | Present work |
| Tb  | 15           | 2.4          | [17]         |
| Dy  | 18           | 5            | [17]         |
| Y   | 15           | –            | [17]         |
| Ho  | 17.8         | 3.5          | [39]         |
| Er  | 15.1         | 4            | Present work |
| Tm  | 14.5         | 5.5          | Present work |

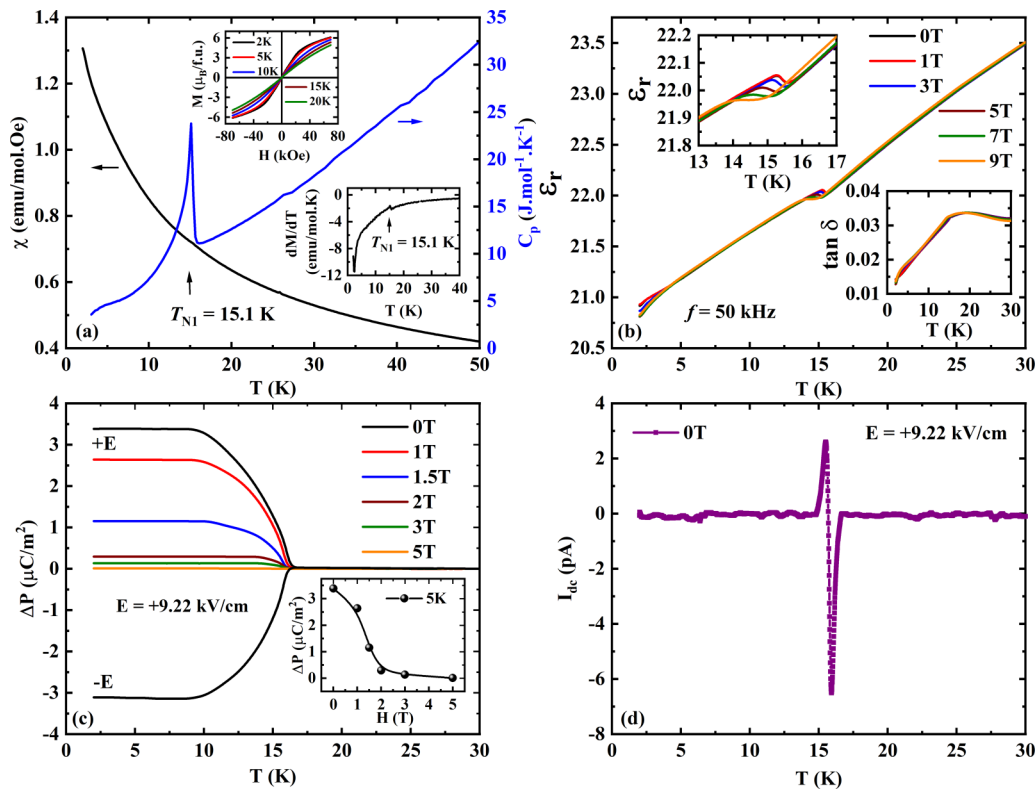


FIG. 7. (a) Left. Temperature evolution of magnetic susceptibility measured under a magnetic field of 0.01 T for ErFeWO<sub>6</sub>. Right. Specific heat data obtained at 0 T. The inset shows isothermal magnetization curves at different temperatures (Top) and  $dM/dT$  vs  $T$  (Bottom). (b) Temperature-dependent dielectric constant recorded under various magnetic fields with frequency  $f = 50$  kHz. The inset shows an enlarged view of dielectric constant (Left) and dielectric loss (Right). (c) Temperature and magnetic field dependence of change in polarization and its switching. The inset shows  $\Delta P$  vs  $H$ . (d) DC bias measurement.

a large magnetization value of  $\sim 7.9 \mu_B/f.u.$ , indicating the ferromagnetic behavior. At the same time, the magnetic moments do not saturate within the experimental limit of 7 T for other compounds suggesting the role of magnetic anisotropy associated with each rare-earth ion. Owing to the rare-earth magnetic anisotropy, the applied magnetic field can change the magnetic state of the rare-earth and thus affect the polarization. The magnetic field-dependent change in polarization reveals the effect of strong  $4f-3d$  interaction in these compounds.

Nevertheless, this is not the case for TmFeWO<sub>6</sub>. From our understanding, there may be no induced moment at the Tm site, and Tm<sup>3+</sup> ions order independently at  $T_{N2} = 5.5$  K. The polarization in the FE1 state is robust against a magnetic field which is similar to YFeWO<sub>6</sub>, whereas the applied magnetic field influences the polarization in the FE2 state [17]. This may be due to a robust antiferromagnetic exchange interaction of Fe<sup>3+</sup> ions, causing the polarization in the FE1 state to be not affected by the applied magnetic fields. Unlike Fe<sup>3+</sup> ordering, the Tm<sup>3+</sup> magnetic order mainly contributes to the polarization in the FE2 state relatively weak and changes easily by the magnetic field. This results in the suppression of polarization under the magnetic fields. Thus, these results indicate that the  $4f-3d$  interaction in TmFeWO<sub>6</sub> is absent or rather weak. Moreover, the polarization in the FE2 state appears well above the  $T_{N2}$  which might be due to the de-

velopment of the antiferromagnetic ordering of Tm<sup>3+</sup> ions at higher temperatures and orders completely at  $T_{N2}$ . In addition to this, the rare-earth cationic size also can be accountable for this behavior. However, one needs to perform neutron diffraction measurements and a single crystal study to validate these arguments.

The paramagnetic space group  $Pna2_1 1'$  is polar and allows the spontaneous electric polarization along the  $z$  direction. However, our PE loop measurements down to liquid nitrogen temperature (77 K) indicates the leaky nature of the samples, as shown in Fig. S20 [38]. Since the cation ordering stabilizes the polar structure at the formation temperature, these compounds do not seem to undergo polar to nonpolar transition, and thus the polarization may not be switchable due to the significant energy barrier between two ferroic states. Nevertheless, all compounds show a change in electric polarization at the magnetic ordering temperature through magnetoelectric coupling.

It should be mentioned here that the change in polarization is significantly less for all the compounds could be due to the polycrystalline nature of the samples measured. Although we did not determine the magnetic structure of these compounds, the emergence of polarization in all four compounds below Fe ordering indicates that these compounds should have the similar noncollinear magnetic structure of Fe spins as that of DyFeWO<sub>6</sub> [17]. The magnetic space group  $C_{2c}$  associated

with the  $\mathbf{k}$  vector  $(0, \frac{1}{2}, \frac{1}{2})$  allows additional polarization along the  $x$  direction with the form  $(P_x, 0, P_z)$ . As discussed in our earlier report, there are two major structural distortions belong to irreps GM1 and GM4 [17]. These modes are responsible for the displacement of O3, O4, and O6 of the paramagnetic structure. This might result in a change in polarization with strong magnetoelectric coupling. It can be possible that these compounds can have independent electric and magnetic orders which strongly coupled through magnetoelastic coupling. However, the mechanism of inverse Dzyaloshinskii-Moriya interaction cannot be neglected since the magnetic structure is noncollinear. Hence, our detailed experimental study reveals that these compounds are magnetically induced multiferroics. The difference in multiferroic properties with each isostructural compound and the magnetic field effect demonstrates the role of  $4f-3d$  interaction along with the rare-earth magnetic anisotropy. Further, it requires a single crystal and neutron diffraction study to understand the magnetoelectric coupling in these compounds.

#### IV. CONCLUSION

In conclusion, we have illustrated the magnetically induced multiferroicity in  $R\text{FeWO}_6$  ( $R = \text{Tm}, \text{Sm}, \text{Gd}$ , and

Er). All these compounds crystallize in polar orthorhombic structure due to the chemical ordering of  $\text{Fe}^{3+}$  and  $\text{W}^{6+}$  ions and exhibit antiferromagnetic order of  $\text{Fe}^{3+}$  ions between  $T_{N1} = 14-18$  K. All these oxides display the field-induced metamagnetic transitions below the rare-earth magnetic ordering temperatures. The dielectric anomalies accompanied by a change in polarization at  $T_{N1}$  evidence the coupling between magnetism and ferroelectricity. Surprisingly, we have observed a second ferroelectric transition at  $T_{N2}$  for  $\text{TmFeWO}_6$ . The influence of magnetic field on the change in polarization indicates the role of the  $4f-3d$  interaction. Hence, the whole aeschynite family of compounds may serve as a playground for studying the multiferroic phenomena and the important role of  $4f-3d$  interaction.

#### ACKNOWLEDGMENT

The authors thank Sheik Saqr Laboratory (SSL) and International Centre for Materials Science (ICMS) at Jawaharlal Nehru Centre for Advanced Scientific Research (JNCASR) for various experimental facilities. A.S. also acknowledges BRICS research project, Department of Science and Technology, Government of India, for a research grant [Sl. No. DST/IMRCD/BRICS/PilotCall2/EMPMM/2018(g)].

- 
- [1] H. Schmid, *Ferroelectrics* **162**, 317 (1994).  
 [2] N. A. Hill, *J. Phys. Chem. B* **104**, 6694 (2000).  
 [3] T. Kimura, T. Goto, H. Shintani, K. Ishizaka, T. Arima, and Y. Tokura, *Nature (London)* **426**, 55 (2003).  
 [4] J. Wang, J. B. Neaton, H. Zheng, V. Nagarajan, S. B. Ogale, B. Liu, D. Viehland, V. Vaithyanathan, D. G. Schlom, and U. V. Waghmare, *Science* **299**, 1719 (2003).  
 [5] N. Hur, S. Park, P. A. Sharma, J. S. Ahn, S. Guha, and S. W. Cheong, *Nature (London)* **429**, 392 (2004).  
 [6] W. Eerenstein, N. D. Mathur, and J. F. Scott, *Nature (London)* **442**, 759 (2006).  
 [7] S.-W. Cheong and M. Mostovoy, *Nat. Mater.* **6**, 13 (2007).  
 [8] D. Khomskii, *Physics* **2**, 20 (2009).  
 [9] Y. Tokura, S. Seki, and N. Nagaosa, *Rep. Prog. Phys.* **77**, 076501 (2014).  
 [10] P. Yanda and A. Sundaresan, in *Advances in the Chemistry and Physics of Materials* (World Scientific, Singapore, 2019), p. 224.  
 [11] D. I. Khomskii, *J. Magn. Magn. Mater.* **306**, 1 (2006).  
 [12] Y. Wang, G. L. Pascut, B. Gao, T. A. Tyson, K. Haule, V. Kiryukhin, and S.-W. Cheong, *Sci. Rep.* **5**, 12268 (2015).  
 [13] Y. S. Oh, S. Artyukhin, J. J. Yang, V. Zapf, J. W. Kim, D. Vanderbilt, and S. W. Cheong, *Nat. Commun.* **5**, 3201 (2014).  
 [14] G. H. Cai, M. Greenblatt, and M. R. Li, *Chem. Mater.* **29**, 5447 (2017).  
 [15] M.-R. Li, P. W. Stephens, M. Retuerto, T. Sarkar, C. P. Grams, J. Hemberger, M. C. Croft, D. Walker, and M. Greenblatt, *J. Am. Chem. Soc.* **136**, 8508 (2014).  
 [16] M.-R. Li, E. E. McCabe, P. W. Stephens, M. Croft, L. Collins, S. V. Kalinin, Z. Deng, M. Retuerto, A. Sen Gupta, H. Padmanabhan, V. Gopalan, C. P. Grams, J. Hemberger, F. Orlandi, P. Manuel, W.-M. Li, C.-Q. Jin, D. Walker, and M. Greenblatt, *Nat. Commun.* **8**, 2037 (2017).  
 [17] S. Ghara, E. Suard, F. Fauth, T. T. Tran, P. S. Halasyamani, A. Iyo, J. Rodríguez-Carvajal, and A. Sundaresan, *Phys. Rev. B* **95**, 224416 (2017).  
 [18] R. Shankar P N, S. Mishra, and A. Sundaresan, *APL Mater.* **8**, 040906 (2020).  
 [19] V. Caignaert, A. Maignan, K. Singh, C. Simon, V. Pralong, B. Raveau, J. F. Mitchell, H. Zheng, A. Huq, and L. C. Chapon, *Phys. Rev. B* **88**, 174403 (2013).  
 [20] T. Kurumaji, S. Ishiwata, and Y. Tokura, *Phys. Rev. X* **5**, 031034 (2015).  
 [21] T. Kurumaji, S. Ishiwata, and Y. Tokura, *Phys. Rev. B* **95**, 045142 (2017).  
 [22] Y. S. Tang, S. M. Wang, L. Lin, C. Li, S. H. Zheng, C. F. Li, J. H. Zhang, Z. B. Yan, X. P. Jiang, and J.-M. Liu, *Phys. Rev. B* **100**, 134112 (2019).  
 [23] M. Li, D. Walker, M. Retuerto, T. Sarkar, J. Hadermann, P. W. Stephens, M. Croft, A. Ignatov, C. P. Grams, and J. Hemberger, *Angew. Chem. Int. Ed.* **52**, 8406 (2013).  
 [24] C. De and A. Sundaresan, *Phys. Rev. B* **97**, 214418 (2018).  
 [25] R. Shankar P N, F. Orlandi, P. Manuel, W. Zhang, P. S. Halasyamani, and A. Sundaresan, *Chem. Mater.* **32**, 5641 13, (2020).  
 [26] R. Salmon, H. Baudry, J. Grannec, G. Le Flem, and F. Sur, *Rev. Chim. Miner.* **11**, 71 (1974).  
 [27] L. Jahnberg, *Acta Chem. Scand.* **17**, 2548 (1963).  
 [28] S. W. Kim, T. J. Emge, Z. Deng, R. Uppuluri, L. Collins, S. H. Lapidus, C. U. Segre, M. Croft, C. Jin, and V. Gopalan, *Chem. Mater.* **30**, 1045 (2018).  
 [29] S. Ghara, F. Fauth, E. Suard, J. Rodríguez-Carvajal, and A. Sundaresan, *Inorg. Chem.* **57**, 12827 (2018).  
 [30] C. Dhital, D. Pham, T. Lawal, C. Bucholz, A. Poyraz, Q. Zhang, R. Nepal, R. Jin, and R. Rai, *J. Magn. Magn. Mater.* **514**, 167219 (2020).



- [31] S. W. Kim, X. Tan, C. E. Frank, Z. Deng, H. Wang, L. Collins, S. H. Lapidus, C. Jin, V. Gopalan, S. V. Kalinin, D. Walker, and M. Greenblatt, *Inorg. Chem.* **59**, 3579 (2020).
- [32] P. Yanda and A. Sundaresan, *Mater. Res. Express* **6**, 124007 (2020).
- [33] Y. Tokunaga, S. Iguchi, T. Arima, and Y. Tokura, *Phys. Rev. Lett.* **101**, 097205 (2008).
- [34] Y. Tokunaga, N. Furukawa, H. Sakai, Y. Taguchi, T. Arima, and Y. Tokura, *Nat. Mater.* **8**, 558 (2009).
- [35] P. Yanda, N. V. Ter-Oganessian, and A. Sundaresan, *Phys. Rev. B* **100**, 104417 (2019).
- [36] P. Yanda, I. V. Golosovsky, I. Mirebeau, N. V. Ter-Oganessian, J. Rodríguez-Carvajal, and A. Sundaresan, *Phys. Rev. Res.* **2**, 023271 (2020).
- [37] J. Rodríguez-Carvajal, in “*Fullprof: A Program for Rietveld Refinement and Pattern Matching Analysis*,” *Abstract of the Satellite Meeting on Powder Diffraction of the XV Congress of the IUCr*, Toulouse, France, 1990, p. 127.
- [38] See Supplemental Material at <http://link.aps.org/supplemental/10.1103/PhysRevMaterials.5.074406> for details on refinement of x-ray diffraction data, inverse susceptibility, dielectric and pyrocurrent measurements.
- [39] M. Adnani, M. Gooch, L. Deng, S. Agrestini, J. Herrero-Martin, H.-C. Wu, C.-K. Chang, T. Salavati-fard, N. Poudel, J. L. García-Muñoz *et al.*, *Phys. Rev. B* **103**, 094110 (2021).
- [40] C. De, S. Ghara, and A. Sundaresan, *Solid State Commun.* **205**, 61 (2015).
- [41] N. Terada, Y. S. Glazkova, and A. A. Belik, *Phys. Rev. B* **93**, 155127 (2016).